

KINETICS OF MARTENSITIC PHASE TRANSITIONS: LATTICE MODEL*

LEV TRUSKINOVSKY[†] AND ANNA VAINCHTEIN[‡]

Abstract. Martensitic phase transitions are often modeled by mixed-type hyperbolic-elliptic systems. Such systems lead to ill-posed initial-value problems unless they are supplemented by an additional kinetic relation. In this paper we explicitly compute an appropriate closing relation by replacing the continuum model with its natural discrete prototype. The procedure can be viewed as either regularization by discretization or a physically motivated account of underlying discrete microstructure. We model phase boundaries by traveling wave solutions of a fully inertial discrete model for a bi-stable lattice with harmonic long-range interactions. Although the microscopic model is Hamiltonian, it generates macroscopic dissipation which can be specified in the form of a relation between the velocity of the discontinuity and the conjugate configurational force. This kinetic relation respects entropy inequality but is not a consequence of the usual Rankine–Hugoniot jump conditions. According to the constructed solution, the dissipation at the macrolevel is due to the induced radiation of lattice waves carrying energy away from the propagating front. We show that sufficiently strong nonlocality of the lattice model may be responsible for the multivaluedness of the kinetic relation and can quantitatively affect kinetics in the near-sonic region. Direct numerical simulations of the transient dynamics suggest stability of at least some of the computed traveling waves.

Key words. martensitic phase transitions, lattice models, nonlocal interactions, driving force, lattice waves, radiative damping

AMS subject classifications. 37K60, 74N10, 74N20, 74H05

DOI. 10.1137/040616942

1. Introduction. A characteristic feature of martensitic phase transitions in active materials is the energy dissipation leading to experimentally observed hysteresis. The dissipation is due to propagating phase boundaries that can be represented at the continuum level as surfaces of discontinuity. Classical elastodynamics admits nonzero dissipation on moving discontinuities but provides no information about its origin and kinetics. Although the arbitrariness of the rate of dissipation does not create problems in the case of classical shock waves, it is known to be the cause of nonuniqueness in the presence of subsonic phase boundaries (see [7, 13, 20] for recent reviews).

The ambiguity at the macroscale reflects the failure of the continuum theory to describe phenomena inside the narrow transition fronts where dissipation actually takes place. The missing closing relation can be found by analyzing a regularized theory which describes the fine structure of the transition front. When the local curvature effects can be neglected, the problem reduces to the study of a one-dimensional steady-state problem. To formulate the simplest problem of this type it is sufficient to consider longitudinal motions of a homogeneous elastic bar. The total energy of

*Received by the editors October 13, 2004; accepted for publication (in revised form) July 22, 2005; published electronically December 30, 2005.

<http://www.siam.org/journals/siap/66-2/61694.html>

[†]Laboratoire de Mécanique des Solides, CNRS-UMR 7649, Ecole Polytechnique, 91128, Palaiseau, France (trusk@lms.polytechnique.fr). The work of this author was supported by NSF grant DMS-0102841.

[‡]Department of Mathematics, University of Pittsburgh, Pittsburgh, PA 15260 (aav4@pitt.edu). The work of this author was supported by NSF grant DMS-0137634.

such bar is the sum of kinetic and potential contributions

$$(1.1) \quad \mathcal{E} = \int \left[\frac{\rho \dot{u}^2}{2} + \phi(u_x) \right] dx,$$

where $u(x, t)$ is the displacement field, $\dot{u} \equiv \partial u / \partial t$ is the velocity, $u_x \equiv \partial u / \partial x$ is the strain, ρ is the constant mass density, and $\phi(u_x)$ is the elastic energy density. The function $u(x, t)$ satisfies the nonlinear wave equation

$$(1.2) \quad \rho \ddot{u} = (\sigma(u_x))_x,$$

where $\sigma(u_x) = \phi'(u_x)$ is the stress-strain relation.

Although in classical elastodynamics (1.2), which is often presented as a first-order p-system, is assumed to be hyperbolic, the hyperbolicity condition $\sigma'(u_x) > 0$ is violated for martensitic materials with nonmonotone stress-strain relation $\sigma(u_x)$ [8]. This makes the initial-value problem associated with the mixed-type equation (1.2) ill-posed; in particular, it leads to the appearance of discontinuities violating the Lax condition (subsonic phase boundaries or kinks, e.g., [16, 17, 31]).

To be more specific, consider a discontinuity moving with velocity V . Let f_- and f_+ denote the limiting values of a function $f(x)$ to the left and to the right of the interface, and introduce the notations $\llbracket f \rrbracket \equiv f_+ - f_-$ for the jump and $\{f\} \equiv (f_+ + f_-)/2$ for the average of f across the discontinuity. The parameters on a discontinuity must satisfy both the classical Rankine–Hugoniot jump conditions,

$$(1.3) \quad \llbracket \dot{u} \rrbracket + V \llbracket u_x \rrbracket = 0, \quad \rho V \llbracket \dot{u} \rrbracket + \llbracket \sigma(u_x) \rrbracket = 0,$$

and the entropy inequality $\mathcal{R} = GV \geq 0$, where

$$(1.4) \quad G = \llbracket \phi \rrbracket - \{ \sigma \} \llbracket u_x \rrbracket$$

is the configurational (driving) force. Contrary to conventional shock waves, the martensitic phase boundaries usually fail to satisfy the Lax condition $c_+ < V < c_-$, where c_{\pm} are the values of the sound velocity in front and behind the discontinuity.

One way to remedy the resulting nonuniqueness is to supplement (1.3) by a *kinetic relation* specifying the dependence of the configurational force on the velocity of the phase boundary $G = G(V)$ [1, 30]. Since the nonlinear wave equation (1.2) provides no information about the kinetic relation, the dependence $G(V)$ has often been modeled phenomenologically [1, 29, 30]. An alternative approach has been to derive the kinetic relation from an augmented model incorporating regularizing terms. A typical example is the viscosity-capillarity model, accounting for both dispersive and dissipative corrections [21, 29]. The problem with both approaches is that they introduce into the theory parameters of unclear physical origin.

The aim of the present paper is to obtain the kinetic relation without any phenomenological assumptions at the macroscale by means of direct replacement of the continuum model (1.2) with its natural discrete prototype. Such procedure of going back from continuum to discrete level can be viewed as either regularization by discretization or as a physically motivated account of underlying atomic or mesoscopic microstructure. It is clear that the discrete model must be Hamiltonian to reproduce the conservative structure of the smooth solutions of (1.2). The energy dissipation on the discontinuities can then be interpreted as the nonlinearity-induced radiation of lattice-scale waves which takes the energy away from the long-wave continuum level. This phenomenon is known in physics literature as radiative damping (e.g., [11, 12]).

To regularize (1.2) from “first principles,” we consider in this paper fully inertial dynamics of a one-dimensional lattice with bi-stability and long-range interactions. Following some previous work on cracks [22] and dislocations [2], we assume piecewise linear approximation of nonlinearity and construct an explicit traveling wave solution of the discrete problem. There exists an extensive literature on shock waves and solitons in the local and nonlocal discrete systems with convex interatomic potentials (e.g., [9, 10, 19, 27]) and on the semilinear prototypes of the present bi-stable system (e.g., [3, 5, 18]). A discrete quasilinear problem for martensitic phase transitions and failure waves in the chains with nearest-neighbor (NN) interactions was considered in [24, 25, 26, 35]. In the present paper we extend these results to the case of harmonic interactions of finite but arbitrary long range. We show that the local (NN) model is degenerate, find a general solution of the nonlocal model, and provide detailed illustrations for a particular case.

Our analytic solutions demonstrate that the nonlocal model generates a much broader class of admissible solutions than the local model; in particular, it allows the possibility of radiation both in front and behind the moving discontinuity. We also show that sufficiently strong nonlocality may be responsible for the multivaluedness of the kinetic relation and can quantitatively affect kinetics in the near-sonic region. The advantage of the explicit formulas obtained in the paper is that they capture certain details that are difficult or even impossible to detect in numerical simulations, such as singular behavior of solutions near static-dynamic bifurcation and around resonances.

The paper is organized as follows. The piecewise linear discrete model with long-range interactions and the associated dynamical system are introduced in section 2. In section 3 we formulate the dimensionless equations for the traveling waves, the boundary conditions, and the admissibility conditions. An explicit solution for the steady state motion of an isolated phase boundary is obtained by Fourier transform in section 4. In section 5 we obtain static solutions describing lattice-trapped phase boundaries and link them to a nontrivial limit of the dynamic solutions. The energy transfer from long to short waves is studied in section 6, where we obtain a closed-form kinetic relation. In section 7 we illustrate the general theory via the case when the only long-range interactions are due to the second nearest neighbors. Numerical simulations of the transient problem suggesting stability of at least sufficiently fast traveling waves are described in section 8. The last section contains our conclusions.

2. Discrete model. The simplest lattice structure can be modeled as a chain of point masses connected by elastic springs. Suppose that the interactions are of long-range type and that every particle interacts with its q neighbors on each side. If $u_n(t)$ is the displacement of the n th particle, the total energy of the chain can be written as

$$(2.1) \quad \mathcal{E} = \varepsilon \sum_{n=-\infty}^{\infty} \left[\frac{\rho \dot{u}_n^2}{2} + \sum_{p=1}^q p \phi_p \left(\frac{u_{n+p} - u_n}{p\varepsilon} \right) \right],$$

where ε is the reference interparticle distance and $\phi_p(w)$ is the energy density of the interaction between p th nearest neighbors. The dynamics of the chain with energy (2.1) is governed by an infinite system of ordinary differential equations:

$$(2.2) \quad \rho \ddot{u}_n = \frac{1}{\varepsilon} \sum_{p=1}^q \left[\phi'_p \left(\frac{u_{n+p} - u_n}{p\varepsilon} \right) - \phi'_p \left(\frac{u_n - u_{n-p}}{p\varepsilon} \right) \right].$$

A continuum system, formally obtained by identifying $u(x, t)$ with a limit of $u(n\varepsilon, t) = u_n(t)$ as $\varepsilon \rightarrow 0$, reduces to the nonlinear wave equation (1.2) with a specific macroscopic stress-strain relation

$$(2.3) \quad \sigma(w) = \sum_{p=1}^q p\phi'_p(w).$$

When the function $\sigma(w)$ is nonmonotone, (1.2) constitutes an incomplete description of the limit. As we show, in this case the correct limit procedure starting from the discrete problem (2.1), (2.2) must also produce a specific kinetic relation $G = G(V)$. This relation, expressed exclusively in terms of the elastic potentials entering (2.1), provides the desired closure for the macroscopic problem (1.2), (1.3). Here we do not consider the issue of a nucleation criterion, whose discrete prototype was studied in [17].

To obtain analytical results, we consider the simplest potentials allowing for a possibility of a phase transitions: bi-quadratic for local interactions (NN) and quadratic for nonlocal interactions (NNN, NNNN, etc.). Specifically we define

$$(2.4) \quad \phi_1(w) = \begin{cases} \frac{1}{2}\Psi(1)w^2, & w \leq w_c, \\ \frac{1}{2}\Psi(1)(w-a)^2 + a\Psi(1)\left(w_c - \frac{a}{2}\right), & w \geq w_c, \end{cases}$$

and

$$(2.5) \quad \phi_p(w) = \frac{1}{2}p\Psi(p)w^2, \quad p = 2, \dots, q.$$

One can see that the nonlinear springs representing NN interactions can be found in two different states depending on whether the strain w is below (phase I) or above (phase II) the critical value w_c . Parameter a defines the microscopic transformation strain (distance between the two linear branches); note that a and w_c are in general independent. For simplicity we assume that the two energy wells of the bi-stable NN potential have equal curvatures $\Psi(1) > 0$.

It is convenient to reformulate the problem using dimensionless variables:

$$(2.6) \quad \bar{t} = t(\Psi(1)/\rho)^{1/2}/\varepsilon, \quad \bar{u}_n = u_n/(a\varepsilon), \quad \bar{w}_c = w_c/a, \quad \bar{\Psi}(p) = \Psi(p)/\Psi(1), \quad p = 1, \dots, q.$$

In terms of these variables with the bars dropped, the energy (2.1) becomes

$$(2.7) \quad \mathcal{E} = \sum_{n=-\infty}^{\infty} \left[\frac{\dot{u}_n^2}{2} - \frac{1}{2} \sum_{|k-n| \leq q} u_n \Psi(k-n) u_k - (u_n - u_{n-1} - w_c) \theta(u_n - u_{n-1} - w_c) \right].$$

By introducing the strain variables $w_n = u_n - u_{n-1}$, we can rewrite the governing equations (2.2) in the form

$$(2.8) \quad \ddot{w}_n - \sum_{|k-n| \leq q} \Psi(k-n) w_k = 2\theta(w_n - w_c) - \theta(w_{n+1} - w_c) - \theta(w_{n-1} - w_c),$$

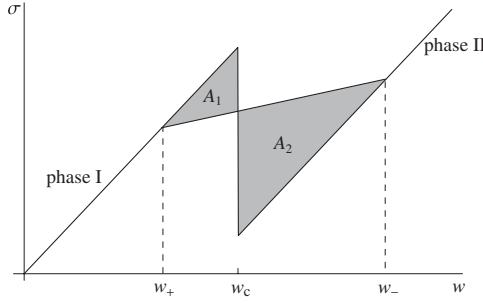


FIG. 2.1. The bi-linear macroscopic stress-strain law and the Rayleigh line connecting the states at infinity for a traveling wave solution describing an isolated phase boundary. The difference between the shaded areas $A_2 - A_1$ represents the configurational force.

where

$$(2.9) \quad \Psi(0) = -2 \sum_{p=1}^q \Psi(p), \quad \Psi(-p) = \Psi(p),$$

and $\theta(w)$ is a unit step function. The macroscopic stress-strain relation (2.3) takes the form

$$(2.10) \quad \sigma(w) = c^2 w - \theta(w - w_c),$$

where

$$(2.11) \quad c = \left(\sum_{p=1}^q p^2 \Psi(p) \right)^{1/2}$$

is the dimensionless macroscopic sound speed. The microscopic elastic moduli $\Psi(p)$ must be chosen to ensure that the uniform deformation $w_n = w$ is stable in each of the phases. For this it is necessary and sufficient that all phonon frequencies $\omega^2(k) > 0$, with $\omega(k)$ defined in (3.6) and $k \in (0, \pi]$, are real. This implies, in particular, that the square of the macroscopic sound speed (2.11) is positive. The resulting macroscopic stress-strain relation (2.10) is shown in Figure 2.1.

3. Traveling waves. An isolated phase boundary moving with a constant velocity V can be obtained as a traveling wave solution of (2.8) with $w_n(t) = w(\xi)$, $\xi = n - Vt$. We assume further that in the moving coordinate system all springs in the region $\xi > 0$ are in phase I ($w_n < w_c$), and all springs with $\xi < 0$ are in phase II. The system (2.8) can then be replaced by a single nonlinear advance-delay differential equation:

$$(3.1) \quad V^2 w'' - \sum_{|p| \leq q} \Psi(p) w(\xi + p) = 2\theta(-\xi) - \theta(-\xi - 1) - \theta(1 - \xi).$$

The configurations at $\xi = \pm\infty$ must correspond to stable homogeneous equilibria plus superimposed short-wave oscillations with zero average; the averaging is over the largest period of oscillations but can be also defined as

$$(3.2) \quad \langle w(\xi) \rangle = \lim_{s \rightarrow \infty} \frac{1}{s} \int_{\xi}^{\xi+s} w(\zeta) d\zeta.$$

In terms of the averaged quantities we obtain the following boundary conditions:

$$(3.3) \quad \langle w(\xi) \rangle \rightarrow w_{\pm} \quad \text{as } \xi \rightarrow \pm\infty.$$

The nonlinearity of the problem is in the switching condition

$$(3.4) \quad w(0) = w_c.$$

We assume that a solution is admissible if the NN springs in front of the moving interface are still in phase I and behind it already in phase II. This implies that

$$(3.5) \quad w(\xi) < w_c \quad \text{for } \xi > 0, \quad w(\xi) > w_c \quad \text{for } \xi < 0.$$

Consequently, the mathematical problem reduces to solving (3.1) subject to (3.3), (3.4), and (3.5).

Observe first that the equation (2.8) is linear in each phase ($\xi < 0$ and $\xi > 0$), which means that the solution can be represented as a superposition of linear waves $w_n = \exp(i(kn - \omega t))$. Since the elastic moduli are equal, the dispersion relation

$$(3.6) \quad \omega^2(k) = 4 \sum_{p=1}^q \Psi(p) \sin^2 \frac{pk}{2}$$

is the same in both phases. For the linear modes to be compatible with the traveling wave ansatz, their phase velocity $V_p(k) = \omega/k$ must be equal to V . This gives the restriction on the admissible wave numbers in the form

$$(3.7) \quad L(k, V) = 0,$$

where

$$(3.8) \quad L(k, V) = 4 \sum_{p=1}^q \Psi(p) \sin^2 \frac{pk}{2} - V^2 k^2.$$

Among the modes selected by (3.7), the ones with complex wave numbers must be exponentially decaying on both sides of the front. They describe the core structure of the phase boundary. The modes with nonzero real wave numbers correspond to radiation. The waves with $k = 0$ are naturally associated with the macroscopic part of the solution.

4. Exact solution. We solve (3.1) by writing $w(\xi) = h(\xi) + w_-$ and applying the complex Fourier transform

$$\hat{h}(k) = \int_{-\infty}^{\infty} h(\xi) e^{i(k+i\alpha)\xi} d\xi, \quad h(\xi) = \frac{1}{2\pi} \int_{-\infty+i\alpha}^{\infty+i\alpha} \hat{h}(k) e^{-ik\xi} dk,$$

where $\alpha > 0$ is a small parameter which guarantees convergence of the integrals. After inverting the Fourier transform and letting $\alpha \rightarrow 0$, we obtain

$$(4.1) \quad w(\xi) = w_- - \frac{2}{\pi i} \int_{\Gamma} \frac{\sin^2(k/2) e^{ik\xi} dk}{kL(k, V)},$$

where the contour Γ coincides with the real axis passing the singular point $k = 0$ from below. The singularities associated with nonzero real roots of $L(k, V) = 0$ must

comply with the radiation conditions. Specifically, the modes with group velocity $V_g = \partial\omega/\partial k$ larger than V can appear only in front, while the modes with $V_g < V$ can appear only behind the phase boundary [24]. Using the relation

$$(4.2) \quad V_g = V + \frac{L_k(k, V)}{2Vk},$$

where $L_k(k, V) = \partial L/\partial k$ and assuming $V > 0$, we obtain that $V_g \geq V$ whenever $kL_k(k, V) \geq 0$. Therefore, to satisfy the radiation conditions, we need to dent the integration contour in (4.1) in such a way that it passes below the singularities on the real axis if $kL_k(k, V) > 0$ and above if $kL_k(k, V) < 0$.

To compute the integral (4.1) explicitly, we use the residue method closing the contour in the upper half-plane when $\xi > 0$ and in the lower half-plane when $\xi < 0$. The solutions look different in the generic case $q > 1$ and the degenerate case $q = 1$.

For $q > 1$ the Jordan lemma can be applied directly, and by separating the macroscopic part of the solution from the microscopic one, we obtain

$$(4.3) \quad w(\xi) = \begin{cases} w_- + \sum_{k \in M^-(V)} \frac{4 \sin^2(k/2) e^{ik\xi}}{kL_k(k, V)} & \text{for } \xi < 0, \\ w_- - \frac{1}{c^2 - V^2} - \sum_{k \in M^+(V)} \frac{4 \sin^2(k/2) e^{ik\xi}}{kL_k(k, V)} & \text{for } \xi > 0. \end{cases}$$

Here

$$(4.4) \quad M^\pm(V) = \{k : L(k, V) = 0, \text{Im}k \geq 0\} \cup N^\pm(V)$$

are all roots of the dispersion relation contributing to the solution on either side of the front, with

$$(4.5) \quad N^\pm(V) = \{k : L(k, V) = 0, \text{Im}k = 0, kL_k(k, V) \geq 0\}$$

denoting the sets of real roots describing radiation.

For $q = 1$ (NN interactions only) the contribution from a semi-arch at infinity does not vanish at $\xi = \pm 0$ and relations (4.3) must be supplemented by the following limiting conditions:

$$(4.6) \quad w(\xi) = \begin{cases} w_- + \sum_{k \in M^-(V)} \frac{4 \sin^2(k/2) e^{ik\xi}}{kL_k(k, V)} - \frac{1}{2} & \text{for } \xi = -0, \\ w_- - \frac{1}{c^2 - V^2} - \sum_{k \in M^+(V)} \frac{4 \sin^2(k/2) e^{ik\xi}}{kL_k(k, V)} + \frac{1}{2} & \text{for } \xi = +0. \end{cases}$$

In both cases, by applying the boundary conditions (3.3) at infinity we obtain

$$(4.7) \quad w_+ = w_- - \frac{1}{c^2 - V^2}.$$

It is easy to see that (4.7) coincides with the Rankine–Hugoniot relation $V^2[[w]] = [[\sigma]]$, computed for the macroscopic stress-strain relation (2.10). The continuity of $w(\xi)$ at $\xi = 0$ implies that

$$(4.8) \quad \frac{1}{c^2 - V^2} + \sum_{k \in M(V)} \frac{4 \sin^2(k/2)}{kL_k(k, V)} = \begin{cases} 1, & q = 1, \\ 0, & q > 1, \end{cases}$$

where $M(V) = M^+(V) \cup M^-(V)$. Condition (4.8) is automatically satisfied for $q > 1$ since the sum of residues at all poles (including $k = 0$) equals zero; for $q = 1$ and $\xi = 0$ the integral over a contour at infinity contributes additional unity in the right-hand side of (4.8). The switching condition (3.4) together with (4.8) requires that

$$(4.9) \quad w_{\pm} = w_c \mp \frac{1}{2(c^2 - V^2)} + \sum_{k \in N_{\text{pos}}(V)} \frac{4 \sin^2(k/2)}{|kL_k(k, V)|},$$

where $N_{\text{pos}}(V) = \{k : L(k, V) = 0, \text{Im}k = 0, k > 0\} \subset M(V)$ is the set of positive real roots of the dispersion relation. By virtue of (4.7), the two conditions (4.9) are dependent and can be replaced by a single condition:

$$(4.10) \quad \frac{1}{2}(w_- + w_+) - w_c = \sum_{k \in N_{\text{pos}}(V)} \frac{4 \sin^2(k/2)}{|kL_k(k, V)|}.$$

As we show in section 6, (4.10) represents the desired kinetic relation.

We can use the explicit formulas for $w(\xi)$ to reconstruct the particle velocity profile from $v(\xi) = -Vw'(\xi)$ if we assume that $V \neq 0$. The relation between the velocity and the strain fields reads

$$(4.11) \quad v(\xi) - v(\xi - 1) = -Vw'(\xi),$$

and the right-hand side is already known from (4.3). Solving (4.11) by Fourier transform, we obtain

$$(4.12) \quad v(\xi) = \begin{cases} v_+ - \frac{V}{c^2 - V^2} - 2V \sum_{k \in M^-(V)} \frac{\sin(k/2)e^{ik(\xi + \frac{1}{2})}}{L_k(k, V)} & \text{for } \xi < -\frac{1}{2}, \\ v_+ + 2V \sum_{k \in M^+(V)} \frac{\sin(k/2)e^{ik(\xi + \frac{1}{2})}}{L_k(k, V)} & \text{for } \xi > -\frac{1}{2}. \end{cases}$$

It is easy to check that the average velocities at infinity satisfy the remaining Rankine–Hugoniot condition (1.3)₁, which in our case takes the form

$$(4.13) \quad v_+ - v_- = \frac{V}{c^2 - V^2}.$$

Notice that the obtained set of traveling wave solutions is parametrized by the velocity V and the boundary value data w_{\pm} and v_{\pm} . The average particle velocity v_+ in front can always be set equal to zero due to the Gallilean invariance. If the strain in front of the discontinuity is also prescribed, the remaining three macroscopic parameters are fully constrained by the two classical Rankine–Hugoniot conditions (4.7) and (4.13), plus the nonclassical admissibility condition (4.10).

5. Static solutions. A special consideration is needed when $V = 0$. In this case continuous variable $\xi = n - Vt$ takes integer values, and the strain profile becomes discontinuous at every $\xi = n$. The differential equation reduces to a system of finite-difference equations, and we can replace the continuous Fourier transform by its discrete analogue (see also [6, 11, 23]). First observe that for a piecewise continuous function $w(\xi)$ with discontinuities at integer ξ we have

$$\hat{w}(k) = \int_{-\infty}^{\infty} w(\xi)e^{ik\xi}d\xi = \sum_{n=-\infty}^{\infty} \int_n^{n+1} w(\xi)e^{ik\xi}d\xi.$$

Therefore, assuming that the strain profile $w(\xi)$ converges to $w_0(n)$ as $V \rightarrow 0$, we obtain

$$(5.1) \quad \hat{w}_0(k) = \sum_{n=-\infty}^{\infty} w_0(n) \frac{e^{ik(n+1)} - e^{ikn}}{ik} = \frac{e^{ik} - 1}{ik} \hat{w}_0^D(k),$$

where $\hat{w}_0^D(k) = \sum_{n=-\infty}^{\infty} w_0(n)e^{ikn}$ is the discrete Fourier transform of $w_0(n)$. Now we can use (4.1) to obtain

$$\hat{w}_0(k) = 2\pi\delta(k)w_- + \frac{4 \sin^2(k/2)}{ik\omega^2(k)},$$

where $\delta(k)$ is the Dirac delta function and $\omega^2(k)$ is given by (3.6). Using (5.1) we can then find $\hat{w}_0^D(k)$ and, applying inverse discrete Fourier transform, obtain a representation of the discrete solution:

$$w_n = \frac{1}{2\pi} \int_{-\pi}^{\pi} \hat{w}_0^D(k) e^{-ikn} dk = w_- - \frac{1}{\pi i} \int_{-\pi}^{\pi} \frac{\sin(k/2) e^{ik(n+1/2)} dk}{\omega^2(k)}.$$

To avoid the singularity at $k = 0$ we must pass it from below; all other roots of the equation $\omega^2(k) = 0$ inside the strip $-\pi \leq \text{Re}k \leq \pi$ have nonzero imaginary parts. Closing the contour of integration in the upper half-plane for $n \geq 0$ and lower half-plane for $n < 0$, we obtain by residue theorem

$$(5.2) \quad w_n = \begin{cases} w_- + \sum_{k \in F^-} \frac{\sin(k/2) e^{ik(n+1/2)}}{\omega(k)\omega'(k)}, & n < 0, \\ w_- - \frac{1}{c^2} - \sum_{k \in F^+} \frac{\sin(k/2) e^{ik(n+1/2)}}{\omega(k)\omega'(k)}, & n \geq 0, \end{cases}$$

where $F^\pm = \{k : \omega^2(k) = 0, \text{Im}k \gtrless 0, -\pi \leq \text{Re}k \leq \pi\}$. Solutions satisfying the admissibility constraints

$$(5.3) \quad w_n \geq w_c \quad \text{for } n \leq -1, \quad w_n \leq w_c \quad \text{for } n \geq 0$$

form a family of lattice-trapped equilibria parametrized by the total stress in the chain $\sigma = c^2 w_- - 1$; the set of such stresses constitutes the *trapping region*.

To specify the trapping region we observe that in our static solutions the phase boundary is pinned at the site $n = -1$. If the strain profile (5.2) is monotone, which occurs, for example, when all long-range interactions are repulsive ($\Psi(p) < 0$ for $p \geq 2^1$), the constraints (5.3) can be replaced by $w_0 \leq w_c$ and $w_{-1} \geq w_c$. The trapping region can then be described explicitly:

$$(5.4) \quad \sigma_M - \sigma_P \leq \sigma \leq \sigma_M + \sigma_P,$$

where $\sigma_M = c^2 w_c - 1/2$ is the Maxwell stress and

$$(5.5) \quad \sigma_P = \frac{1}{2} + c^2 \sum_{k \in F^+} \frac{\sin(k/2) e^{ik/2}}{\omega(k)\omega'(k)}$$

¹Since $\Psi(1) = 1 > 0$, the homogeneous phases can still be stable if the negative long-range moduli are sufficiently small.

is the *Peierls stress* (see also [4, 32]). The phase boundary remains trapped until the stress reaches one of the limiting values: $\sigma = \sigma_M - \sigma_P$, corresponding to $w_{-1} = w_c$ when the interface starts moving to the left ($V < 0$), or $\sigma = \sigma_M + \sigma_P$, corresponding to $w_0 = w_c$ when the interface starts moving to the right ($V > 0$). The two limiting solutions represent unstable equilibria from which the dynamic solution bifurcates.

6. Kinetic relation. The waves generated in the core of the moving phase boundary carry the energy away from the front without changing the average values of parameters at infinity. At the continuum level these lattice waves are invisible and therefore the associated energy transfer is perceived as dissipation. To evaluate the rate of dissipation, we start with the microscopic energy balance

$$\frac{d\mathcal{E}}{dt} = \mathcal{A}(t),$$

where \mathcal{E} is the total energy of the chain and $\mathcal{A}(t)$ is the power supplied by the external loads. Since the solution of the discrete problem at infinity can be represented as a sum of the macroscopic contribution and the superimposed oscillations, we can split the averaged power accordingly. We obtain

$$(6.1) \quad \langle \mathcal{A} \rangle = \mathcal{P} - \mathcal{R},$$

where $\mathcal{P} = \sigma_+ v_+ - \sigma_- v_-$ is the macroscopic rate of work and \mathcal{R} is the energy release due to radiated waves which is invisible at the macroscale. While in the general case the expression for \mathcal{R} may contain coupling terms, in the piecewise linear model adopted in this paper, the macroscopic and microscopic contributions decouple (see also [11, 24]). The dissipation rate \mathcal{R} can be written as the sum of the contributions from the areas ahead and behind the front:

$$(6.2) \quad \mathcal{R}(V) = \mathcal{R}_+(V) + \mathcal{R}_-(V).$$

To specify the entries in the right-hand side, we observe that due to the exponential decay of the modes with complex wave numbers, the strain and velocity fields given by (4.3) and (4.12) have the following asymptotic representation at $\xi = \pm\infty$:

$$v(\xi) \approx v_0(\xi) + \sum_{k \in N_{\text{pos}}(V)} v_k(\xi), \quad w(\xi) \approx w_0(\xi) + \sum_{k \in N_{\text{pos}}(V)} w_k(\xi),$$

where

$$v_0(\xi) = \begin{cases} v_-, & \xi < 0, \\ v_+, & \xi > 0, \end{cases} \quad w_0(\xi) = \begin{cases} w_-, & \xi < 0, \\ w_+, & \xi > 0, \end{cases}$$

are the homogeneous components and

$$(6.3) \quad v_k(\xi) = \begin{cases} -\frac{4V \sin(k/2) \cos(k(\xi - 1/2))}{L_k(k, V)}, & \xi < 0, k \in N_{\text{pos}}^-(V), \\ \frac{4V \sin(k/2) \cos(k(\xi - 1/2))}{L_k(k, V)}, & \xi > 0, k \in N_{\text{pos}}^+(V), \end{cases}$$

$$w_k(\xi) = \begin{cases} \frac{8 \sin^2(k/2) \cos k\xi}{kL_k(k, V)}, & \xi < 0, k \in N_{\text{pos}}^-(V), \\ -\frac{8 \sin^2(k/2) \cos k\xi}{kL_k(k, V)}, & \xi > 0, k \in N_{\text{pos}}^+(V), \end{cases}$$

are the oscillatory components. Here $N_{\text{pos}}^{\pm}(V) \equiv \{k \in N^{\pm}(V) : k > 0\}$ (recall (4.5)), $N_{\text{pos}}^+(V) \cup N_{\text{pos}}^-(V) = N_{\text{pos}}(V)$. Due to the asymptotic orthogonality of the linear modes, the terms in the right-hand side of (6.2) can be expressed as contributions due to individual modes. Since the energy flux associated with the linear mode k is the product of the average energy density $\langle \mathcal{G}_k \rangle$ and the relative velocity $|V_g - V|$ of the energy transport with respect to the moving front, we can write

$$(6.4) \quad \mathcal{R}_+(V) = \sum_{k \in N_{\text{pos}}^+(V)} \langle \mathcal{G}_k \rangle_+(V_g - V), \quad \mathcal{R}_-(V) = \sum_{k \in N_{\text{pos}}^-(V)} \langle \mathcal{G}_k \rangle_-(V - V_g).$$

Here $\langle \mathcal{G}_k \rangle_{\pm}$ is the average energy density carried by the wave with the wave number $k \in N_{\text{pos}}^{\pm}(V)$. It is given by

$$\begin{aligned} \langle \mathcal{G}_k \rangle_{\pm} = & \lim_{n \rightarrow \pm\infty} \frac{1}{2V\tau(k)} \int_{n-V\tau(k)}^n \left[v_k^2(\xi) + c^2(w_k(\xi))^2 \right. \\ & \left. - \sum_{p=1}^{q-1} B(p) \{ (w_k(\xi+p) - w_k(\xi))^2 + (w_k(\xi) - w_k(\xi-p))^2 \} \right] d\xi, \end{aligned}$$

where $B(p) = \frac{1}{2} \sum_{l=1}^{q-p} l\Psi(l+p)$ and $\tau(k) = 2\pi/\omega(k) = 2\pi/(Vk)$. Using (6.3), we obtain

$$\langle \mathcal{G}_k \rangle_{\pm} = \frac{8V^2 \sin^2(k/2)}{(L_k(k, V))^2},$$

which gives for the total energy flux

$$\mathcal{R}(V) = \sum_{k \in N_{\text{pos}}^+(V)} \frac{4V \sin^2(k/2)}{kL_k(k, V)} - \sum_{k \in N_{\text{pos}}^-(V)} \frac{4V \sin^2(k/2)}{kL_k(k, V)} = \sum_{k \in N_{\text{pos}}(V)} \frac{4V \sin^2(k/2)}{|kL_k(k, V)|}.$$

Recalling the definition $\mathcal{R}(V) = G(V)V$ we can write the microscopic expression for the configurational force:

$$(6.5) \quad G(V) = \sum_{k \in N_{\text{pos}}(V)} \frac{4 \sin^2(k/2)}{|kL_k(k, V)|}.$$

The function $G(V)$ is well-defined since both $L(k, V)$ and $N_{\text{pos}}(V)$ depend on V in a known way. Comparing (6.5) with the macroscopic definition of the configurational force (1.4) we obtain

$$(6.6) \quad G = \frac{1}{2}(w_- + w_+) - w_c,$$

which can be interpreted geometrically as the area difference between two shaded triangles in Figure 2.1. Combining (6.5) and (6.6), we obtain exactly (4.10), which shows that (4.10) is indeed the desired kinetic relation and that micro and macro assessments of dissipation are compatible.

7. An example. To illustrate the general solution, consider a special case $q = 2$ (see Figure 7.1). The model is then fully characterized by a single dimensionless parameter,

$$\beta = 4\Psi(2)/\Psi(1),$$

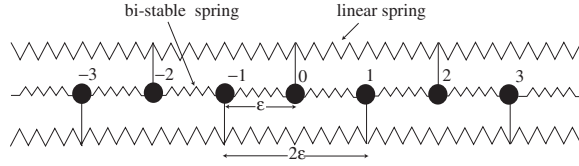


FIG. 7.1. Discrete chain with nearest and next-to-nearest-neighbor interactions ($q = 2$).

measuring the relative strength of NNN and NN interactions. The stability constraints (e.g., [36]) give $-1 < \beta \leq \infty$. Recalling that the inequality $\Psi(2) < 0$ is suggested by the linearization of the potentials of the Lennard–Jones type [32, 33], we can further restrict the admissible interval to

$$(7.1) \quad -1 < \beta \leq 0.$$

The total energy of the system can be written as

$$(7.2) \quad \mathcal{E} = \sum_{n=-\infty}^{\infty} \left[\frac{w_n^2}{2} + \frac{1 + \beta}{2} w_n^2 - \theta(w_n - w_c)(w_n - w_c) - \frac{\beta}{4} (w_{n+1} - w_n)^2 \right].$$

One can see that parameter $\beta/(1 + \beta)$ characterizes the effect of discreteness: $\beta \sim 0$ corresponds to weak and $\beta \sim -1$ to strong coupling. This identification is compatible with the fact that at $\beta = 0$ the Peierls stress characterizing the size of the lattice-trapping domain takes the largest value (equal to the spinodal limit), while at $\beta = -1$ the Peierls stress is equal to zero.²

The energy (7.2) produces the following equation for the traveling waves:

$$(7.3) \quad V^2 w'' - \frac{\beta}{4} \left(w(\xi + 2) - 2w(\xi) + w(\xi - 2) \right) - w(\xi + 1) + 2w(\xi) - w(\xi - 1) = 2\theta(-\xi) - \theta(-\xi - 1) - \theta(1 - \xi).$$

The formal solution of this equation has been obtained in section 4. Below we provide detailed illustrations for the physically relevant range of parameters β .

7.1. Dispersion relation. To compute the strain and velocity profiles at a given V we need to find the nonzero roots k of the dispersion relation

$$(7.4) \quad L(k, V) = 4 \sin^2(k/2) + \beta \sin^2 k - V^2 k^2 = 0.$$

It is convenient to present the complex roots explicitly as $k = k_1 + ik_2$ and divide them into three categories: real, responsible for radiation; purely imaginary, providing the monotone structure of the core region; and complex with nonzero real part, describing oscillatory contributions to the core.

Since $L(k, V)$ is an even function of k , the real roots appear in pairs $k = \pm k_1$. Assuming positive V , we obtain

$$V(k_1) = \frac{\sqrt{4 \sin^2(k_1/2) + \beta \sin^2 k_1}}{|k_1|}.$$

This function is plotted in Figure 7.2(a). An infinite number of local maxima on

²The picture emerging in our piecewise linear model is somewhat obscured by the fact that in the limit of strong coupling the macroscopic sound speed tends to zero.

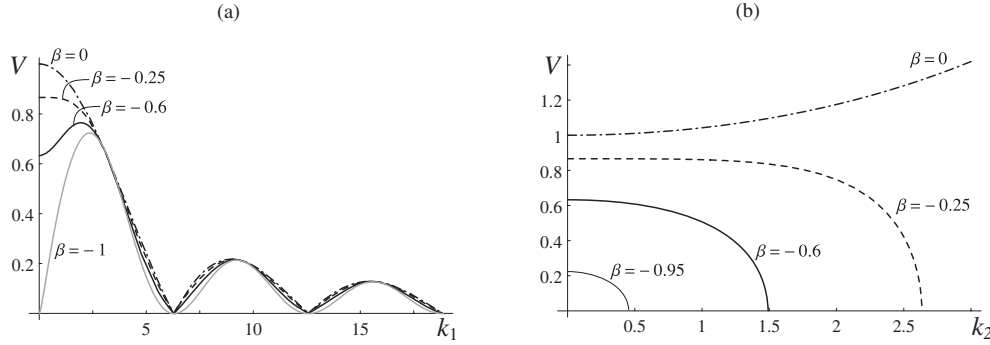


FIG. 7.2. Real (a) and imaginary (b) roots of the dispersion relation $L(k, V) = 0$ at different β .

this graph, denoted by $V = V_i$, correspond to resonance velocities: at these points $L_k(k, V) = 0$ and the sums in (4.3), (4.9), and (4.12) diverge. Between the resonance velocities, (7.4) possesses a finite number of positive real roots corresponding to propagating waves. To determine whether these waves propagate ahead or behind the front, we need to check whether $kL_k(k, V) = 2k^3V(k)V'(k)$ is positive or negative. At $V > 0$ the radiation conditions say that the waves with $kV'(k) > 0$ propagate in front of the phase boundary, while the waves with $kV'(k) < 0$ propagate behind.

Changing β affects the function $V(k)$ noticeably only at long waves (small k). A straightforward computation shows that $V(0)$ is equal to the macroscopic sound speed $c = (1 + \beta)^{1/2}$. We also obtain that $V'(0) = 0$ and

$$V''(0) = -\frac{1 + 4\beta}{12\sqrt{1 + \beta}}.$$

At $-1/4 < \beta \leq 0$, the function $V(k)$ has a maximum at $k = 0$ while at $-1 < \beta < -1/4$ it has a local minimum implying that sufficiently strong coupling ($\beta < -1/4$) creates the possibility for the lattice waves to move faster than the macroscopic sound speed. The range of supersonic speeds increases as $\beta \rightarrow -1$, and in the limiting case $\beta = -1$ all propagating waves are macroscopically supersonic. It is interesting that the critical value $\beta = -1/4$ also emerges in the strain-gradient approximation of the energy (7.2), where it corresponds to the change of sign of the coefficient in front of the strain gradient term [15, 28]. In this approximation the dispersion relation $V(k)$ is replaced by a parabola: for $\beta > -1/4$ (weak nonlocality) the parabola is directed downward and the strain-gradient coefficient is negative while for $\beta < -1/4$ (strong nonlocality) the parabola is upward and the strain-gradient contribution to the energy is positive definite. The latter implies that subsonic phase boundaries can only be dissipation free. To yield a nontrivial kinetic relation in this range of parameters the quasicontinuum model must be augmented by higher-order terms [37].

The purely imaginary roots of (7.4) appear in symmetric pairs and correspond to nonoscillatory modes exponentially decreasing away from the front. By solving $L(ik_2, V) = 0$ for V we obtain

$$V(k_2) = \frac{\sqrt{4 \sinh^2(k_2/2) + \beta \sinh^2 k_2}}{|k_2|}.$$

This function is shown in Figure 7.2b. One can show that $V(0) = c$, $V'(0) = 0$, and $V''(0) = (1 + 4\beta)/(12\sqrt{1 + \beta})$. For $-1 < \beta < -1/4$ the maximum of the curve

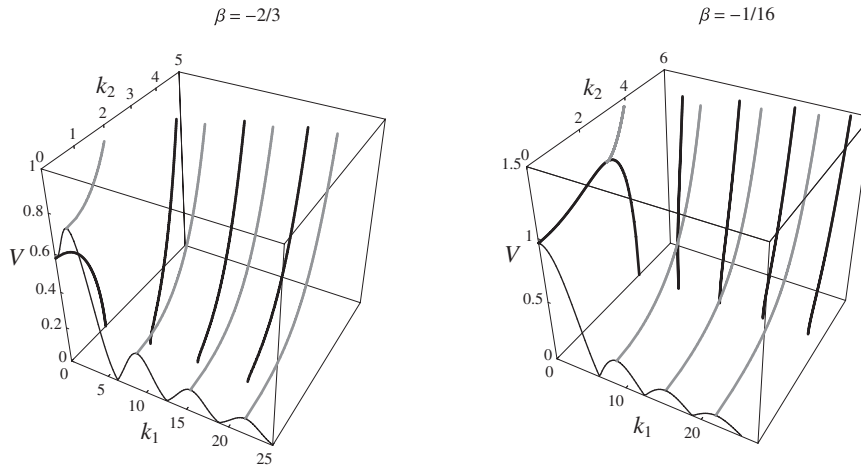


FIG. 7.3. The structure of nonzero roots of $L(k, V) = 0$ in the cases of strong ($\beta = -2/3$) and weak ($\beta = -1/16$) nonlocality. Thin lines: real roots, set N ; thick lines: P -roots; gray lines: Q -roots.

$V(k_2)$ is reached at $k_2 = 0$, which means that in the case of strong coupling only macroscopically subsonic phase boundaries have monotone contribution to the core structure. Both the value $V(0)$ and the range of available wave numbers decrease as $\beta \rightarrow -1$, so that in the limit purely imaginary roots disappear. In the case $\beta = 0$ the function $V(k_2)$ is convex and no imaginary roots contribute to the subsonic solution. This is compatible with the fact that in the degenerate NN limit the static interface ($V = 0$) is atomically sharp.

Complex roots with nonzero real part contribute to the oscillatory structure of the core region. For the given V the real (k_1) and imaginary (k_2) parts of the relevant wave numbers satisfy the system of two equations: $\text{Re}L(k_1 + ik_2, V) = 0$ and $\text{Im}L(k_1 + ik_2, V) = 0$. The set of complex roots contains infinitely many branches that come in symmetric quadruples. The first quadrant of the complex plane is shown in Figure 7.3. The complex roots can be divided into two sets: Q and P . The set Q (thick gray lines), has a purely dynamic nature and contributes to the boundary layers around the front only at nonzero V . The set P , shown in Figure 7.3 by thick black lines, contains purely imaginary branches which intersect the plane $V = 0$ and contribute to the static solution: at $V = 0$ they are given by

$$(7.5) \quad k = 2\pi n \pm i\lambda, \quad \lambda = 2\text{arccosh} \left[\frac{1}{\sqrt{|\beta|}} \right],$$

where n is an integer [33]. As β tends to zero, the imaginary parts of P -roots approach $\pm\infty$; the eventual disappearance of these roots in the limit $\beta \rightarrow 0$ is responsible for the sharpening of the front in the NN approximation.

7.2. Strain and velocity profiles. Typical profiles of strain $w(\xi)$ and velocity $v(\xi)$ computed for the NNN model from (4.3), (4.12) are shown in Figure 7.4, where $\beta = -0.2$. For this case the first two resonance velocities are $V_1 = 0.2164$ and $V_2 = 0.1282$. Accordingly, at $V = 0.5 > V_1$ we see only one radiative mode propagating behind the phase boundary; at $V_2 < V = 0.16 < V_1$ the solution exhibits two additional radiative modes, one propagating behind and one in front of the phase boundary.

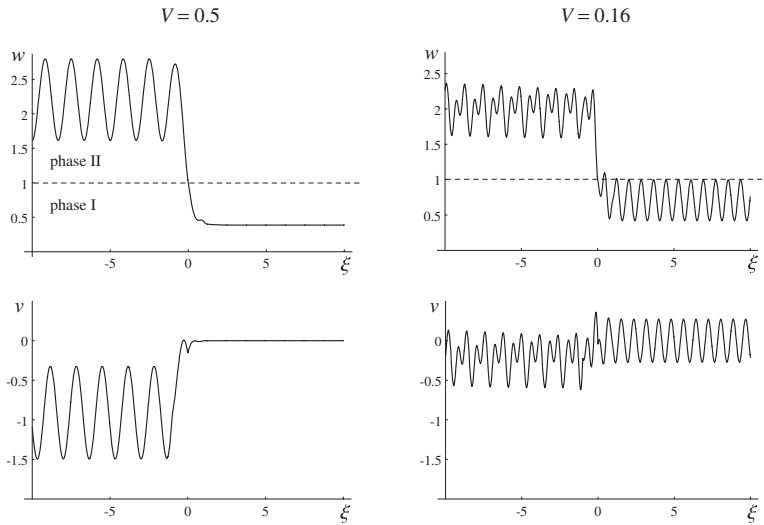


FIG. 7.4. Strain and velocity profiles at $V > V_1$ and $V_2 < V < V_1$. Here $\beta = -0.2$, $w_c = 1$, $v_+ = 0$.

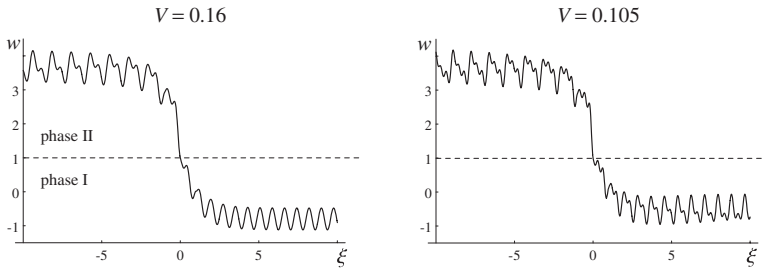


FIG. 7.5. Strain profiles at $V_2 < V < V_1$ and $V_3 < V < V_2$. Here $\beta = -0.75$, $w_c = 1$.

A closer inspection of the solutions at $V < 0.266$ reveals a violation of the constraints (3.5): in the strain profile corresponding to $V = 0.16$ in Figure 7.4 the threshold $w = w_c$ is crossed at both $\xi = 0$ and $\xi > 0$. Moreover, for this value of β our numerical computations suggest that the entire velocity interval $(0, 0.266)$ around the resonances has to be excluded as inadmissible. Similar “velocity gaps” also have been detected in [11, 12, 14] for the semilinear Frenkel–Kontorova problem.

At larger β steady interface propagation becomes possible in certain subcritical velocity intervals. For instance, at $\beta = -0.75$ we found admissible traveling wave solutions in the intervals: $[0.24, 0.5]$ (between $V_1 = 0.215$ and $c = 0.5$); $[0.142, 0.19]$ (between V_1 and $V_2 = 0.1279$); $[0.1, 0.11]$ (between V_2 and $V_3 = 0.0912$); $[0.078, 0.08]$ (between V_3 and $V_4 = 0.0708$); and possibly in some shorter intervals at smaller V . Two such solutions are shown in Figure 7.5. The first one corresponds to $V = 0.16$, which is between the first and second resonances; unlike its counterpart at $\beta = -0.2$, this solution is admissible. The second admissible profile corresponds to the value of velocity $V = 0.105$ located between the second and third resonances. In this case there are five radiative modes, two in front and three behind the phase boundary. The appearance of the small-velocity intervals of existence of the traveling wave solutions

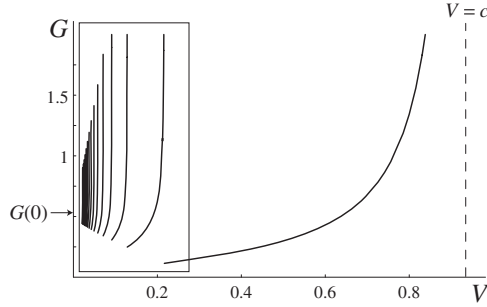


FIG. 7.6. Kinetic relation $G(V)$ for $\beta = -1/8$. The region inside the rectangle should be excluded because the corresponding solutions violate admissibility constraints (3.5).

at nonzero β is due to the presence of P -roots at nonzero β : as β grows in absolute value, these roots move closer to the real axis, widening the transition layer and suppressing oscillations due to the Q -roots (see Figure 7.3).

7.3. Kinetic relation. Using (6.5) and the known dispersion spectrum, we can now explicitly evaluate the kinetic relation $G(V)$. A representative example is shown in Figure 7.6. At resonance velocities the configurational force required to move the interface tends to infinity. The singularities are due to equal curvatures of the energy wells ensuring that the energy transport is simultaneously blocked in both phases. The main physical reasons are related to low dimensionality of the model and the absence of microscopic dissipation.

As we discussed above, at sufficiently small β the entire region around the small-velocity resonances has to be excluded because the corresponding solutions violate the admissibility constraints (3.5). With β increasing, some of the small-velocity solutions between the resonances become admissible, as shown in Figure 7.7(b)–(d). Observe also that there is an infinite number of β at which the sonic speed c coincides with one of the resonance velocity. Thus, at $\beta = -0.9539$ we have $c = V_1 = 0.2147$, implying that for $\beta \leq -0.9539$ the subsonic region lies below the first resonance (see Figure 7.7(d)). Overall, the total domain of existence of the traveling wave solutions shrinks as $\beta \rightarrow -1$, while the domain of admissible traveling waves between the resonances expands.

Zero-velocity limit. To check the compatibility of static and dynamic branches of solutions it is instructive to trace the zero velocity limit of our dynamic theory. At $V = 0$ we can use (5.2) with $F^\pm = \{\pm i\lambda\}$, where λ is defined in (7.5). After some algebraic manipulations, the family of lattice-trapped equilibria (5.2) can be represented in the form

$$(7.6) \quad w_n = \begin{cases} \frac{\sigma + 1}{1 + \beta} - \frac{e^{\lambda(n+1/2)}}{2(1 + \beta) \cosh(\lambda/2)}, & n < 0, \\ \frac{\sigma}{1 + \beta} + \frac{e^{-\lambda(n+1/2)}}{2(1 + \beta) \cosh(\lambda/2)}, & n \geq 0, \end{cases}$$

where σ lies in the region (5.4). The solutions (7.6) can be shown to be metastable [32]. The expression for the Peierls stress (5.5) marking the threshold of metastability can now be written explicitly as

$$\sigma_P = \frac{1}{2} \sqrt{1 + \beta}.$$

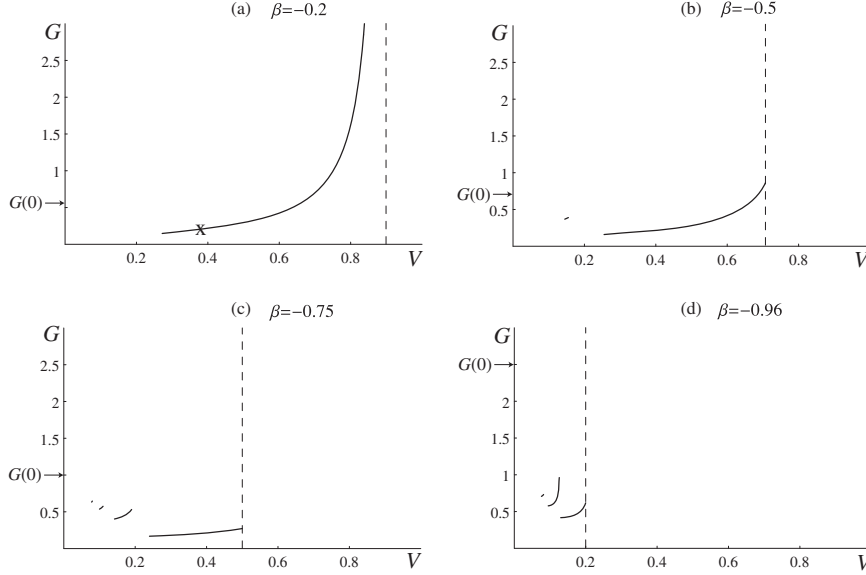


FIG. 7.7. Kinetic relations $G(V)$ for different β . The point marked by x in (a) corresponds to the numerical results in Figures 8.1 and 8.2.

Observe that at $\beta = 0$ the Peierls stress coincides with the spinodal stress $\sigma_S = 1/2$. As β grows, the trapping region becomes narrower and eventually disappears at $\beta = -1$ ($\sigma_P = 0$). The upper boundary of the trapping region (5.4) corresponds to the case when $w_0 = w_c$, which is exactly the condition (3.4). The corresponding saddle-point configuration is given by

$$(7.7) \quad w_n = \lim_{V \rightarrow 0} w(n - Vt) = \begin{cases} w_c + \frac{e^{\lambda/2} - e^{\lambda(n+1/2)}}{2(1 + \beta) \cosh(\lambda/2)}, & n < 0, \\ w_c + \frac{e^{-\lambda(n+1/2)} - e^{-\lambda/2}}{2(1 + \beta) \cosh(\lambda/2)}, & n \geq 0. \end{cases}$$

Using this solution, we can obtain the value of the configurational force at the depinning limit:

$$(7.8) \quad G(0) = \frac{1}{2}(w_- + w_+) - w_c = \frac{1}{2\sqrt{1 + \beta}}.$$

Notice that although the Peierls stress tends to zero when $\beta \rightarrow -1$, the corresponding value of the configurational force $G(0)$ tends to infinity. This is, of course, an artifact of our specific assumptions concerning the elastic moduli and is due to the divergence of the macroscopic transformation strain in the limit.

Sonic limit. The qualitative behavior of the function $G(V)$ in the limit $V \rightarrow c$ depends on β . If $-1/4 < \beta \leq 0$, and $V \lesssim c$, the wave spectrum contains a single wave number k which approaches zero as $V \rightarrow c$. Expanding the expression for the configurational force (6.5) at small k we obtain

$$G \sim \frac{6}{(1 + 4\beta)k^2},$$

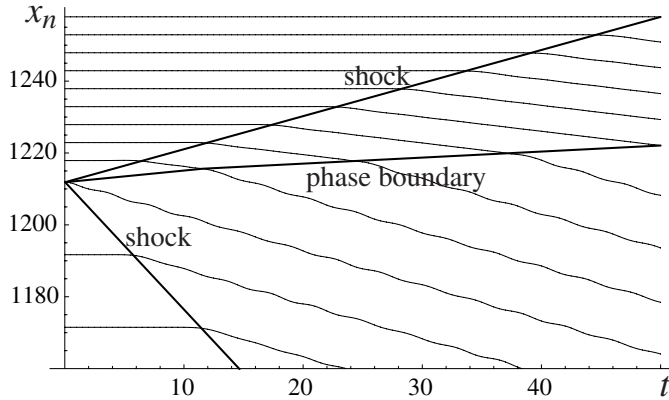


FIG. 8.1. Positions $x_n(t)$ of every fifth particle in the interval $290 \leq n \leq 345$ in numerical solution of the Riemann problem with initial data compatible with the traveling wave at $V = 0.375$ at $\beta = -0.2$. The phase boundary is initially placed at $n_0 = 300$, and the problem is solved on the interval $1 \leq n \leq 600$. The corresponding point on the kinetic relation $G(V)$ is marked by x in Figure 7.7a.

which implies that $G(V) \rightarrow \infty$ as $V \rightarrow c$ (see Figures 7.6 and 7.7(a)). The picture is qualitatively different when $-1 < \beta < -1/4$. In this case as V approaches c from below, the limit of the corresponding real wave number k is nonzero k_s , and therefore configurational force $G(V)$ remains finite (see Figure 7.7(b)–(d)).

8. Stability of the traveling waves. We now present some numerical experiments aimed at accessing stability of the admissible traveling wave solutions. To simplify the consideration of the transient regimes for the system (2.8), we consider Riemann initial data of the form

$$(8.1) \quad (w_n, v_n)|_{t=0} = \begin{cases} (w_-^0, 0), & n < n_0, \\ (w_c, 0), & n = n_0, \\ (w_+^0, 0), & n > n_0. \end{cases}$$

We assume that $w_+^0 < w_c$ and $w_-^0 > w_c$. The analysis of the corresponding continuum problem for the p-system (1.2) suggests the formation of a phase boundary with two shocks in front and behind (e.g., [17]). This is indeed what we see in Figure 8.1, which shows a typical numerical solution of (2.8) obtained using the Verlet algorithm on a large domain.

After a transient period, the phase boundary starts moving with a constant speed. To check convergence of the non-steady-state problem to the admissible traveling wave solution we used the following algorithm. For a traveling wave solution with velocity V , (4.9) provides the average strains at both sides of the discontinuity $w_{\pm}(V)$. We can then use (4.13) and the Rankine–Hugoniot jump conditions across the shocks to compute the corresponding initial strains w_{\pm}^0 in terms of V and v_+ . Without loss of generality, we choose v_+ so that $w_+^0 = 0$ and obtain an explicit formula relating the Riemann data with the observed phase boundary velocity:

$$w_-^0(V) = w_-(V) + w_+(V) + \frac{V}{c(c^2 - V^2)} = 2 \left(w_c + \sum_{k \in N_{\text{pos}}(V)} \frac{4 \sin^2(k/2)}{|kL_k(k, V)|} \right) + \frac{V}{c(c^2 - V^2)}.$$

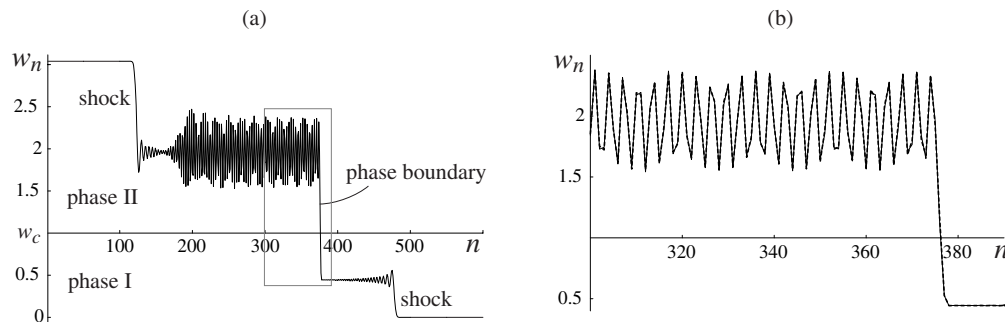


FIG. 8.2. (a) Strain profile $w_n(200)$ for the numerical solution shown in Figure 8.1. (b) The same solution (solid line) zoomed in around the phase boundary (inside the rectangle in (a)) and compared to the analytical traveling wave solution (thick dashed line).

Computations based on this relation consistently indicate that the fast branch of the kinetic relation ($V > V_1$) corresponds to traveling wave solutions with a finite domain of attraction. An example corresponding to $\beta = -0.2$ and $V = 0.375$ is shown in Figures 8.1 and 8.2. One can see not only that the generated phase boundary propagates steadily with the predicted velocity but that the strain profile $w_n(t)$ zoomed around the phase boundary (solid line in Figure 8.2(b)) compares perfectly with the analytical solution (4.3) (thick dashed line). The above analysis suggests that the fast branch of the kinetic relation with $V > V_1$, corresponding to traveling wave solutions with a single oscillatory mode behind and monotonic leading edge, is locally stable; proving this conjecture rigorously is highly nontrivial.

Unfortunately, we were not able to find similar evidence of numerical stability for admissible traveling waves with $V < V_1$ exhibiting oscillations both behind and in front of the phase boundary. Numerical simulation for the data expected to converge to the particular traveling wave lead instead to a solution which does not agree with the traveling wave ansatz although the phase boundary propagates steadily (with a slightly smaller velocity). The macroscopic solution is very close to the corresponding traveling wave; the analytical formula captures the core structure but not the oscillations. One can conjecture that while an admissible traveling wave with radiation on both sides of the front is not a global attractor, it is surprisingly close to one.

Finally, we refer to [17] for a related study of the phase boundary stability in the context of a different discretization of the mixed-type p-system.

9. Conclusions. In this paper we used a physically motivated discretization of the p-system to derive an explicit kinetic relation for a one-dimensional theory of martensitic phase transitions. The macroscopic dissipation was interpreted as the energy of the lattice waves emitted by a moving macroscopic discontinuity. By using the simplest piecewise linear model, we obtained an explicit formula for the continuum rate of entropy production which depends only on interatomic potentials. We showed that despite the difference in the structure of micro and macro theories, the assessments of dissipation at different scales are fully compatible. The present study complements previous analyses of related systems in fracture and plasticity framework by including general harmonic long-range interactions.

More specifically, we showed that contrary to the simplest theory with NN interactions, which has a mean field character and is therefore degenerate, strongly nonlocal models produce multivalued kinetic relations with several admissible branches and

rich variety of configurations of emitted lattice waves. In addition to enlarging the domain of existence of steady-state regimes, sufficiently strong long-range interactions significantly alter the structure of mobility curves near sonic speeds. The nonlocality also affects the size of lattice trapping: as long-range interactions become stronger, the trapping region reduces in size in terms of stress. At the same time, it widens in our model in terms of driving forces, which emphasizes an important difference between the physical and configurational descriptions. Although the main effects of nonlocality were illustrated in the paper by the explicit computations for the NNN model, we have also conducted a similar study of the NNNN model which showed qualitatively similar behavior.

The present work was motivated by similar studies of the semilinear discrete Frenkel–Kontorova model (e.g., [11, 12]). While the two models turn out to be equivalent in static and overdamped limits [32, 34], the fully inertial versions are quite different. An additional level of complexity in the quasilinear model considered here is associated with a different structure of nonlinearity that results in the presence of the limiting characteristic velocity, microscopic and macroscopic particle velocities, and the discrete Rankine–Hugoniot jump conditions.

REFERENCES

- [1] R. ABEYARATNE AND J. KNOWLES, *A continuum model of a thermoelastic solid capable of undergoing phase transitions*, J. Mech. Phys. Solids, 41 (1993), pp. 541–571.
- [2] W. ATKINSON AND N. CABRERA, *Motion of a Frenkel-Kontorova dislocation in a one-dimensional crystal*, Phys. Rev. A, 138 (1965), pp. 763–766.
- [3] O. M. BRAUN AND Y. S. KIVSHAR, *Nonlinear dynamics of the Frenkel-Kontorova model*, Phys. Rep., 306 (1998), pp. 1–108.
- [4] O. M. BRAUN, Y. S. KIVSHAR, AND I. I. ZELENKAYA, *Kinks in the Frenkel-Kontorova model with long-range interparticle interactions*, Phys. Rev. B, 41 (1990), pp. 7118–7138.
- [5] A. CARPIO AND L. L. BONILLA, *Oscillatory wave fronts in chains of coupled nonlinear oscillators*, Phys. Rev. E, (2003), p. 056621.
- [6] V. CELLI AND N. FLYTZANIS, *Motion of a screw dislocation in a crystal*, J. Appl. Phys., 41 (1970), pp. 4443–4447.
- [7] C. M. DAFERMOS, *Hyperbolic Conservation Laws in Continuum Physics*, Springer-Verlag, Heidelberg, 2000.
- [8] J. ERICKSEN, *Equilibrium of bars*, J. Elasticity, 5 (1975), pp. 191–202.
- [9] Y. GAIDIDEIB, N. FLYTZANIS, A. NEUPERA, AND F. G. MERTENSA, *Effect of non-local interactions on soliton dynamics in anharmonic chains: Scale competition*, Phys. D, 107 (1997), pp. 83–111.
- [10] T. Y. HOU AND P. LAX, *Dispersive approximations in fluid dynamics*, Comm. Pure Appl. Math., 44 (1991), pp. 1–40.
- [11] O. KRESSE AND L. TRUSKINOVSKY, *Mobility of lattice defects: Discrete and continuum approaches*, J. Mech. Phys. Solids, 51 (2003), pp. 1305–1332.
- [12] O. KRESSE AND L. TRUSKINOVSKY, *Lattice friction for crystalline defects: From dislocations to cracks*, J. Mech. Phys. Solids, 52 (2004), pp. 2521–2543.
- [13] P. G. LEFLOCH, *Hyperbolic Systems of Conservation Laws*, ETH Lecture Note Series, Birkhäuser, Boston, 2002.
- [14] M. MARDER AND S. GROSS, *Origin of crack tip instabilities*, J. Mech. Phys. Solids, 43 (1995), pp. 1–48.
- [15] R. D. MINDLIN, *Second gradient of strain and surface tension in linear elasticity*, Internat. J. Solids Structures, 1 (1965), pp. 417–438.
- [16] S.-C. NGAN AND L. TRUSKINOVSKY, *Thermal trapping and kinetics of martensitic phase boundaries*, J. Mech. Phys. Solids, 47 (1999), pp. 141–172.
- [17] S.-C. NGAN AND L. TRUSKINOVSKY, *Thermo-elastic aspects of dynamic nucleation*, J. Mech. Phys. Solids, 50 (2002), pp. 1193–1229.
- [18] M. PEYRARD, *Simple theories of complex lattices*, Phys. D, 123 (1998), pp. 403–424.

- [19] M. PEYRARD, S. PNEVMATIKOS, AND N. FLYTZANIS, *Discreteness effects on non-topological kink soliton dynamics in nonlinear lattices*, Phys. D, 19 (1986), pp. 268–281.
- [20] D. SERRE, *Systems of Conservation Laws*, vols. 1, 2, Cambridge University Press, Cambridge, UK, 1999.
- [21] M. SLEMROD, *Admissibility criteria for propagating phase boundaries in a van der Waals fluid*, Arch. Ration. Mech. Anal., 81 (1983), pp. 301–315.
- [22] L. I. SLEPYAN, *Dynamics of a crack in a lattice*, Soviet Phys. Dokl., 26 (1981), pp. 538–540.
- [23] L. I. SLEPYAN, *The relation between the solutions of mixed dynamical problems for a continuous elastic medium and a lattice*, Soviet Phys. Dokl., 27 (1982), pp. 771–772.
- [24] L. I. SLEPYAN, *Models and Phenomena in Fracture Mechanics*, Springer-Verlag, New York, 2002.
- [25] L. I. SLEPYAN, A. CHERKAEV, AND E. CHERKAEV, *Transition waves in bistable structures. II. Analytical solution: wave speed and energy dissipation*, J. Mech. Phys. Solids, 53 (2005), pp. 407–436.
- [26] L. I. SLEPYAN AND L. V. TROYANKINA, *Fracture wave in a chain structure*, J. Appl. Mech. Tech. Phys., 25 (1984), pp. 921–927.
- [27] M. TODA, *Theory of nonlinear lattices*, Springer-Verlag, Berlin, 1989.
- [28] N. TRIANTAFYLIDIS AND S. BARDENHAGEN, *The influence of scale size on the stability of periodic solids and the role of associated higher order gradient continuum models*, J. Mech. Phys. Solids, 44 (1996), pp. 1891–1928.
- [29] L. TRUSKINOVSKY, *Equilibrium interphase boundaries*, Soviet Phys. Dokl., 27 (1982), pp. 306–331.
- [30] L. TRUSKINOVSKY, *Dynamics of nonequilibrium phase boundaries in a heat conducting elastic medium*, J. Appl. Math. Mech., 51 (1987), pp. 777–784.
- [31] L. TRUSKINOVSKY, *Kinks versus shocks*, in IMA Series in Mathematics and Its Applications, E. D. R. Fosdick and M. Slemrod, eds., Vol. Math. Appl. 52, Springer-Verlag, 1993, pp. 185–229.
- [32] L. TRUSKINOVSKY AND A. VAINCHTEIN, *Peierls-Nabarro landscape for martensitic phase transitions*, Phys. Rev. B, 67 (2003), p. 172103.
- [33] L. TRUSKINOVSKY AND A. VAINCHTEIN, *The origin of nucleation peak in transformational plasticity*, J. Mech. Phys. Solids, 52 (2004), pp. 1421–1446.
- [34] L. TRUSKINOVSKY AND A. VAINCHTEIN, in preparation.
- [35] L. TRUSKINOVSKY AND A. VAINCHTEIN, *Explicit kinetic relation from “first principles,”* in Advances in Mechanics and Mathematics, vol. 11, P. Steinmann and G. Maugin, eds., Springer, New York, 2005.
- [36] L. TRUSKINOVSKY AND A. VAINCHTEIN, *Quasicontinuum modeling of short-wave instabilities in crystal lattices*, Philosophical Magazine, to appear.
- [37] L. TRUSKINOVSKY AND A. VAINCHTEIN, *Quasicontinuum models of dynamic phase transitions*, Continuum Mechanics and Thermodynamics, submitted.